

JP3.1 6 TROPICAL CYCLONE INDUCED TORNADES ASSOCIATED WITH THE FORMATION OF TROPICAL STORM BARRY

Andrew Devanas* and Kennard B. Kasper
NOAA/National Weather Service, Key West, Florida

Dan Gregoria and Pablo Santos
NOAA/National Weather Service, Miami, Florida

1. INTRODUCTION

Tropical Storm Barry developed from a tropical depression which originated around 1200 UTC 1 June 2007 over the extreme southeastern Gulf of Mexico, just northwest of the western tip of Cuba (Avila 2007), and approximately 425 km west-southwest of Key West, Florida. The depression intensified during the next six hours as it moved north at near 5 m s^{-1} , becoming Tropical Storm Barry at 1800 UTC over the southeastern Gulf of Mexico (Fig. 1). The tropical cyclone intensified further during the afternoon, with peak intensity reached at 0000 UTC 2 June (minimum central MSL pressure of 997 hPa; maximum sustained winds of 25 m s^{-1}) when the system was centered about 240 km west-southwest of the Dry Tortugas.

Two tornadoes associated with Tropical Storm Barry were confirmed over southern Florida during the afternoon and evening of 1 June. An EF0 tornado moved across portions of northern Sugarloaf Key in the lower Florida Keys of Monroe County at about 1650 UTC, and an EF1 tornado moved over portions of Cutler Ridge in southeastern Miami-Dade County at 0150 UTC 2 June. Both tornadoes developed in association with mini supercells (Burgess et al. 1995). Additional mini supercells were identified by both Key West and Miami Weather Surveillance Radar-1988 Doppler (WSR-88D) during the afternoon and evening of 1 June with no subsequent tornado reports.

The tornadoes and mini supercells of 1 June developed within the northeastern Cartesian quadrant and right-front sector (relative to system translation vector) of Tropical Storm Barry. This quadrant and sector have been identified in previous studies as having an overall favorable shear profile with respect to the other quadrants/sectors, and is climatologically the most favored region for tropical cyclone-induced tornadogenesis (Smith 1965; Pearson and Sadowski 1965; Hill et al. 1966; Novlan and Gray 1974; Gentry 1983; and McCaul 1991). McCaul (1991) has identified this region of a tropical cyclone as favorable for mini supercells and tornadoes owing to the typically highly sheared and weakly buoyant lower troposphere.

Tornadoes and mini supercells developed near a weak, synoptic-scale baroclinic zone which was drawn

northward from the western Caribbean basin in the increasing southerly low-level flow east of incipient Tropical Storm Barry. The NCEP Global Forecast System (GFS) 6-h forecast valid at 0600 UTC 1 June depicts the boundary south of the Florida Keys in Fig. 2. This boundary was apparently very important in creating an environment favorable for tornadogenesis by introducing a zone of enhanced vertical wind shear and concentrated vorticity while also transporting maritime tropical air northward, thereby increasing potential buoyant energy in the lower troposphere across southern Florida. The boundary moved northward during the day on 1 June as Tropical Storm Barry evolved, reaching southern peninsular Florida by 0000 UTC 2 June. Similar synoptic-scale boundaries have been documented with past hybrid and tropical cyclone tornado outbreaks in Florida (Hagemeyer and Matney 1993; Edwards and Pietrycha 2006).

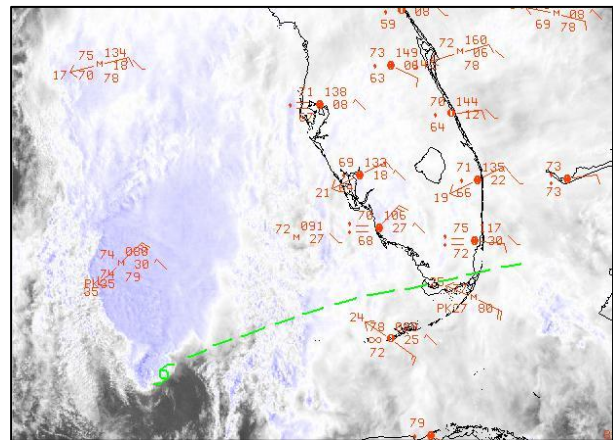


Fig. 1. Tropical Storm Barry visible satellite image at 2100 UTC 1 Jun 2007. Green dashed line shows approximate position of surface boundary extending from the center of the storm over southern Florida.

Lower-tropospheric storm-relative helicity (SRH) increased substantially across all of southern Florida and adjoining waters throughout the day on 1 June in the wake of the aforementioned boundary, with peak 0–3-km SRH values near $350 \text{ m}^2 \text{ s}^{-2}$. A distinct horizontal buoyancy gradient was noted across the boundary, with surface based convective available potential energy (SBCAPE) around 400 J kg^{-1} in advance of the boundary, increasing to in excess of 1500 J kg^{-1} well south of the boundary by the late afternoon and evening.

Operational warning forecasters are often challenged by subtle radar signatures embedded in complex and busy radar fields during tropical cyclones. Spratt et al.

* Corresponding author address: Andrew Devanas,
NOAA/National Weather Service, 1315 White Street,
Key West, FL 33040; e-mail: andrew.devanas@noaa.gov

(1997) found small reflectivity cores (greater than 50 dBZ) coincident with storm-relative rotational velocities of 6–15 m s⁻¹ useful in tropical cyclone tornado detection. These cells persisted for 1–2 hours and displayed shear values of 0.010 s⁻¹ near time of tornado occurrence. Schneider and Sharp (2006) studied 15 tropical cyclone spawned tornadoes, three of which were associated with rotation at or above the 1.5-degree elevation angle prior to tornado sightings. They also pointed out three radar signatures which provided “good lead time”: near gate-to-gate rotational velocity (V_r) of 10 m s⁻¹ or greater; a hook or appendage signature in reflectivity data; and the presence of a (base) velocity enhancement signature (VES) of 15 m s⁻¹ or greater between 2.1 and 4.3 km AGL.

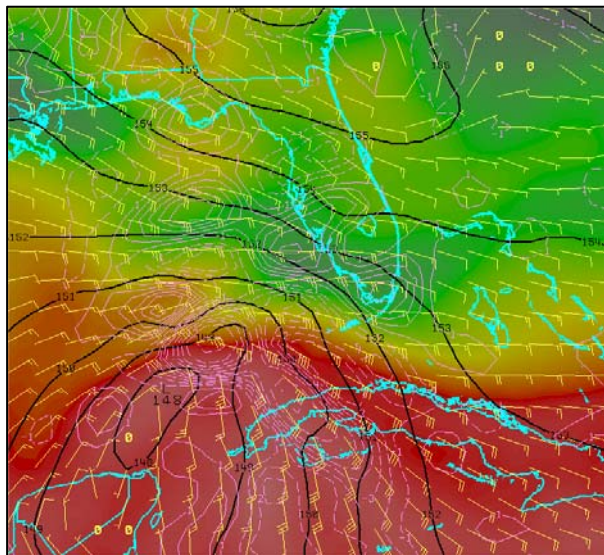


Fig. 2. NCEP GFS 6-h forecast (valid at 0600 UTC 1 Jun 2007) of 850-hPa geopotential height (black solid line), divergence (pink dashed line), wind (yellow barbs), and equivalent potential temperature (image).

The purpose of this study is to present an analysis of the pre-storm and near-storm environments of the southern Florida tornadoes of 1–2 June 2007 in the context of past research, with an emphasis on metrics (particularly on the storm scale) available in an operational warning environment.

2. METHODOLOGY

The WSR-88D data from both Key West (KBYX) and Miami (KAMX) were archived for 1–2 June 2007. The data were then loaded into the Weather Event Simulator (WES) for analysis. The WES is a workstation-based system designed to simulate the Advanced Weather Information Processing System (AWIPS) workstations used operationally in National Weather Service Forecast Offices.

The following criteria were required for a convective cell to be considered for more rigorous storm-scale

analysis: a) rotational velocity at the lowest elevation scan (0.5°) of 5 m s⁻¹ or greater; b) circulation evident through at least the two lowest elevation scans; c) mesocyclone diameter <5.6 km (3 n mi); d) criteria in a–c persisted through at least three consecutive volume scans. Five discrete convective cells were examined based on these criteria, including those that spawned the Sugarloaf and Cutler Ridge tornadoes. The associated mesocyclones identified in storm-scale radar analysis are hereinafter referred to by the following names: Sugarloaf; Big Pine; Everglades; Card Sound; and Cutler Ridge, based on their respective locations. Figure 3 identifies the mesocyclone locations (red labels) from southwest to northeast across southern Florida. The Sugarloaf and Big Pine mesocyclones occurred during the early afternoon in the lower Florida Keys, within 30 km of each other. The Everglades, Card Sound, and Cutler Ridge mesocyclones all occurred during the evening in the vicinity of southeastern Miami-Dade County. The Big Pine, Everglades, and Card Sound mesocyclones tracked over water or unpopulated land, whereas the Sugarloaf and Cutler Ridge tornadoes occurred in populated areas, rendering their identification by the public much more likely.

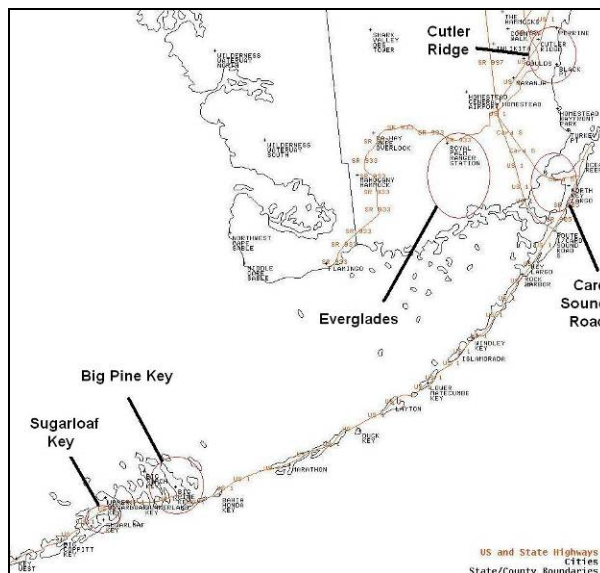


Fig. 3. Map of extreme southern tip of the Florida peninsula and the Florida Keys illustrating the locations of the mesocyclones evaluated in this paper.

The radar-derived parameters of reflectivity, rotational velocity (V_r), rotational shear (S_r), mesocyclone depth, mesocyclone persistence, vertical wind profile, and SRH were examined at the storm scale during the life cycle of each cell. Other radar fields were also inspected to determine their utility in identifying cells or cell families which warranted examination at the storm scale in an operational environment. These fields will be referred to as discriminators. The cell discriminators examined were VES, Spectrum Width (SW), and Digital Vertical Integrated Liquid (DVL). The

SW was mentioned by both Spratt et al. (1997) and Pfost (2002) as a useful cell discriminator, especially for cells at greater distances from the radar.

3. RESULTS

3.1 Near-Storm Environment/Boundary Identification

The northward movement of a synoptic-scale boundary and subsequent increase in both potential buoyancy and storm-relative environmental helicity over southern Florida are easily discerned through a temporal comparison of parameters derived from Key West and Miami rawinsonde observations (raobs) taken at 1200 UTC 1 June and 0000 UTC 2 June. The Key West raob at 1200 UTC revealed a SBCAPE of 242 J kg^{-1} , while the Miami raob showed a SBCAPE of 0 J kg^{-1} . The 0000 UTC 2 June Key West and Miami raobs revealed SBCAPEs of 1875 J kg^{-1} and 360 J kg^{-1} , respectively. Winds below 850 hPa over southern Florida were mainly easterly north of the boundary, veering to the southeast and then south as the boundary passed. Figure 4 shows a time series of wind velocity from the surface to 3 km AGL at the NOAA Environmental Technology Laboratory (ETL) profiler site on Cudjoe Key, located just east of Sugarloaf Key, within 5 km of the Sugarloaf tornado path. Examination of these point data shows the change in the 0–1-km winds around 1700 UTC at Cudjoe Key (the Sugarloaf tornado occurred around 1650 UTC). In addition, a spatial analysis of surface winds and radar reflectivity over southern Florida and adjacent coastal waters (Fig. 5) confirms a shear zone associated with the northward-moving boundary.

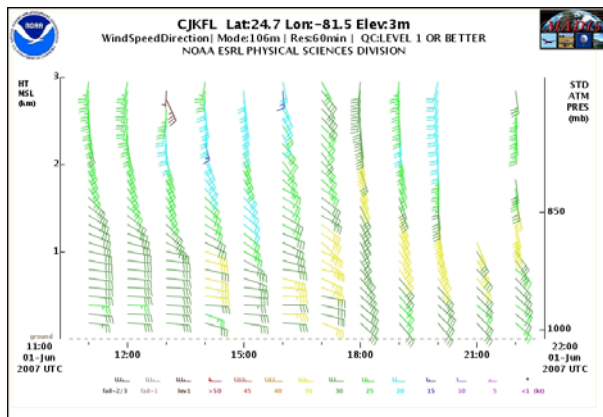


Fig. 4. A time-height section of wind velocity, 1000–2200 UTC, 1 Jun 2007, from the NOAA/ETL Profiler, Cudjoe Key, Florida. Full wind barbs indicate wind speeds of 5 m s^{-1} .

The Key West and Miami raobs are again revealing, showing a substantial increase in SRH and subsequent high potential for rotating convective cells. At Key West, a 0–1-km (0–3-km) SRH of $71 \text{ m}^2 \text{ s}^{-2}$ ($280 \text{ m}^2 \text{ s}^{-2}$) was observed at 1200 UTC 1 June, while at 0000 UTC 2 June, the 0–1-km (0–3-km) SRH had increased to $183 \text{ m}^2 \text{ s}^{-2}$ ($283 \text{ m}^2 \text{ s}^{-2}$). Substantial increases in SRH were

also observed at Miami where a 0–1-km (0–3-km) SRH of $-7 \text{ m}^2 \text{ s}^{-2}$ ($144 \text{ m}^2 \text{ s}^{-2}$) was observed at 1200 UTC 1 June, and a 0–1-km (0–3-km) SRH of $259 \text{ m}^2 \text{ s}^{-2}$ ($358 \text{ m}^2 \text{ s}^{-2}$) was observed at 0000 UTC 2 June.

The Sugarloaf and Big Pine mesocyclones developed along the leading edge of the northward-moving boundary, while the Everglades, Card Sound, and Cutler Ridge mesocyclones developed just south of the boundary. The boundary at the surface is clearly evident in the in the KBYX 0.5° reflectivity field shown in Fig. 5 (white oval). The reflectivity image is from 1655 UTC, which is during the Sugarloaf tornado (just north of the white arrow).

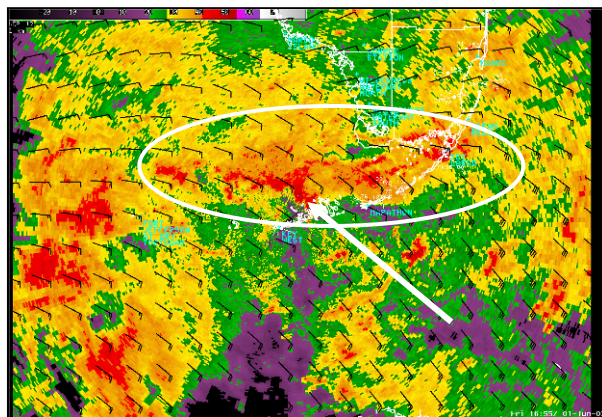


Fig. 5. KBYX 0.5° -degree base reflectivity image at 1655 UTC 1 Jun 2007 with a Local Analysis and Prediction Scheme (LAPS) surface wind analysis overlay. Full wind barbs indicate wind speeds of 5 m s^{-1} .

3.2 Reflectivity Analysis

Figures 6–8 show base reflectivity signatures of the Sugarloaf, Big Pine, and Everglades mesocyclones, respectively, near the time of maximum V_r and S_r . Figure 9 shows the Card Sound (south) and Cutler Ridge (north) mesocyclones, also near time of maximum V_r and S_r .

The Sugarloaf and Big Pine mesocyclones were analyzed using KBYX radar data, and the Everglades, Card Sound, and Cutler Ridge mesocyclones were analyzed using KAMX radar data. All images are base reflectivity images from the lowest elevation slice (0.5°). The KBYX radar was operating in Volume Coverage Pattern (VCP) 12, while the KAMX radar was operating in VCP 121. At the 0.5° elevation angle all mesocyclones contained reflectivity cores $>50 \text{ dBZ}$, with inner cores around 55 dBZ . These mesocyclone core reflectivities tended to be of higher value than those associated with nearby non-mesocyclonic cells.

All mesocyclones exhibited weak echo regions (WER) near the reflectivity cores, with the exception of the Big Pine mesocyclone (Fig. 7). It was difficult to detect a WER with certainty in the Big Pine

mesocyclone at any point. However, it will be shown that while the lowest level circulation of the Big Pine mesocyclone was as strong as the others in the study, it was also the shallowest mesocyclone. Moreover, the Big Pine mesocyclone also had the shortest lifespan. These factors likely contributed to the lack of organization in the reflectivity field.

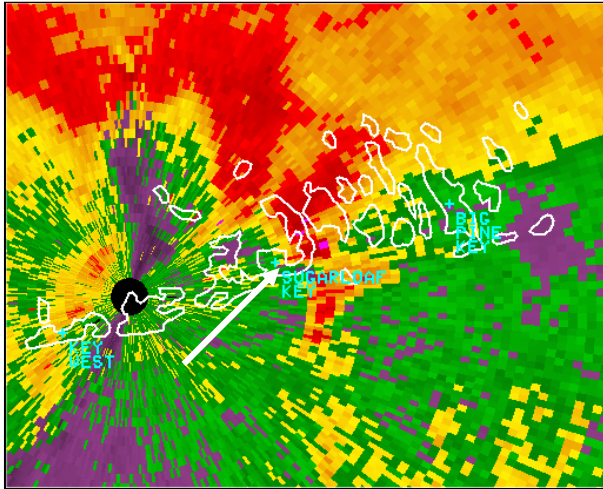


Fig. 6. KBYX 0.5-degree base reflectivity image at 1647 UTC 1 Jun 2007; Sugarloaf mesocyclone denoted by white arrow.

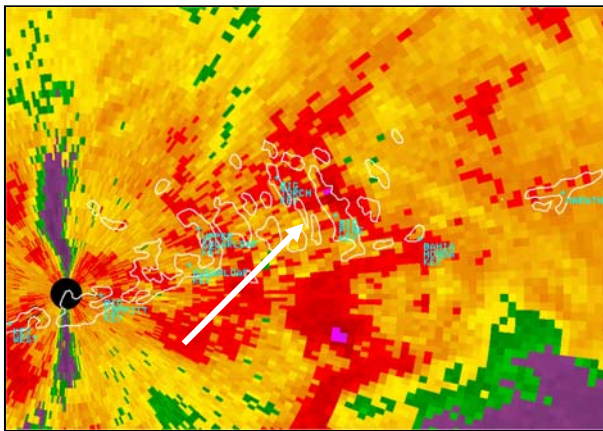


Fig. 7. KBYX 0.5-degree base reflectivity image at 1609 UTC 1 Jun 2007; Big Pine mesocyclone denoted by white arrow.

The Sugarloaf (Fig. 6), Everglades (Fig. 8), and Card Sound (Fig. 9) mesocyclones each exhibited a classic hook appendage adjacent and to the right of the reflectivity core during maximum strength.

The Cutler Ridge (Fig. 9) mesocyclone had an appendage to the southeast of the reflectivity core, but displayed more of a “kidney bean” appearance (forward flank notch) than a hook echo. An appendage could not be found in the Big Pine mesocyclone.

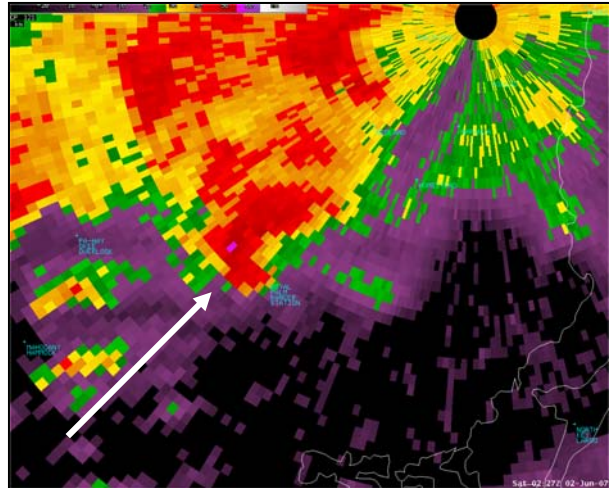


Fig. 8. KAMX 0.5-degree base reflectivity image at 0227 UTC 2 Jun 2007; Everglades mesocyclone denoted by white arrow.

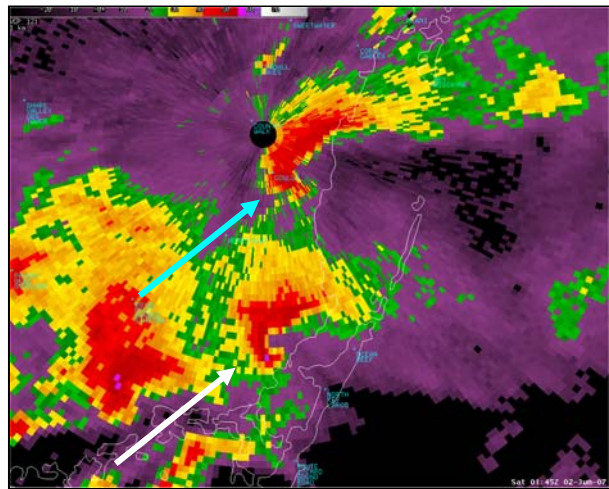


Fig. 9. KAMX 0.5-degree base reflectivity image at 0145 UTC 2 Jun 2007; Card Sound (Cutler Ridge) mesocyclone denoted by white (blue) arrow.

3.3 Rotational Velocity (V_r), Rotational Shear (S_r), Depth of Mesocyclone

The rotational velocity, shear, and depth of each mesocyclone were measured for each volume scan as long as the mesocyclone maintained a measureable circulation (as defined in Section 2). Figures 10-14 show these parameters as a function of time for each mesocyclone. The S_r has been multiplied by 10^3 for plotting convenience.

A vertical green line has been added to the Sugarloaf and Cutler Ridge plots to denote the approximate time of reported tornado occurrences. With the exception of the Big Pine cell, the mesocyclone lifespan averaged 1–3 hours, consistent with results from previous research (Spratt et al. 1997). Also, the longer-duration mesocyclones exhibited a cyclic pattern with respect to overall cell intensity. However, sample size is not large

enough to draw statistical conclusions concerning cycle periodicity. The Big Pine and Cutler Ridge mesocyclones briefly re-appeared after having become untraceable for several scans (not shown).

The Big Pine mesocyclone average depth was only 1.3 km, while the average depth of the remaining four mesocyclones was 3.0 km. The Sugarloaf, Card Sound, and Cutler Ridge mesocyclones decreased in depth as they intensified.

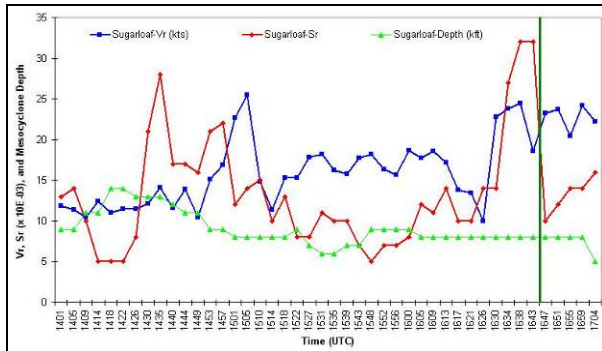


Fig. 10. Sugarloaf mesocyclone, 1401-1704 UTC 1 Jun 2007. V_r , S_r , and mesocyclone depth.

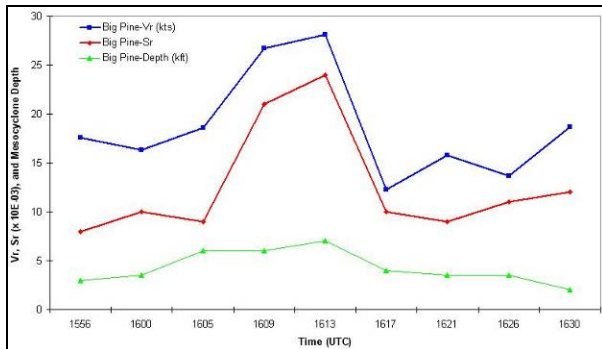


Fig. 11. Big Pine mesocyclone, 1555-1630 UTC 1 Jun 2007. V_r , S_r , and mesocyclone depth.

The V_r and S_r for all mesocyclones averaged 9 m s^{-1} and 0.012 s^{-1} , respectively. Separating the Sugarloaf and Cutler Ridge mesocyclones (which spawned the two confirmed tornadoes), and averaging the 10 volume scans nearest reported tornado occurrence, the values of V_r and S_r increase slightly to 9.4 m s^{-1} and 0.014 s^{-1} .

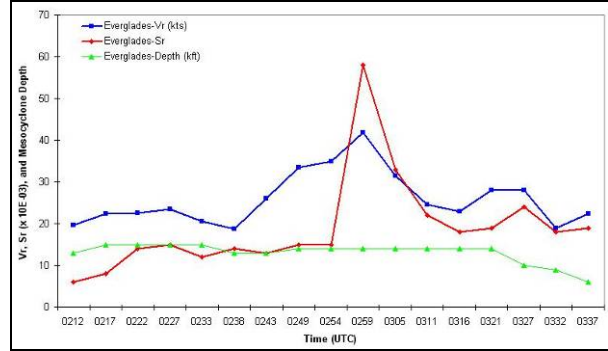


Fig. 12. Everglades mesocyclone, 0212-0337 UTC 2 Jun 2007. V_r , S_r , and mesocyclone depth.

The highest V_r and S_r occurred with the Everglades mesocyclone at 0259 UTC 2 June, with a V_r of 21.5 m s^{-1} and S_r of 0.058 s^{-1} . The Sugarloaf mesocyclone showed the most organization of the five in the study, with the longest lifespan. During one 17-min stretch (1630 to 1647 UTC), gate-to-gate shear was analyzed through 1.8 km. The mesocyclone weakened just prior to landfall on Sugarloaf Key around 1650 UTC.

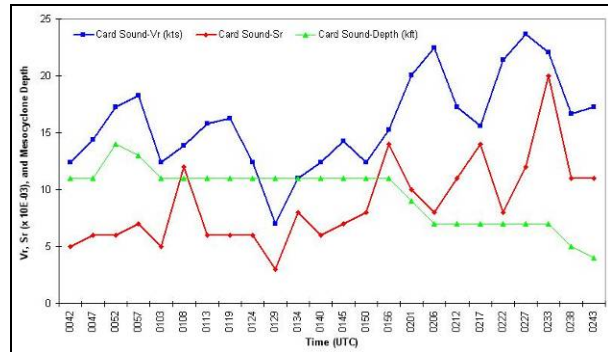


Fig. 13. Card Sound mesocyclone, 0042-0243 UTC 2 Jun 2007. V_r , S_r , and mesocyclone depth.

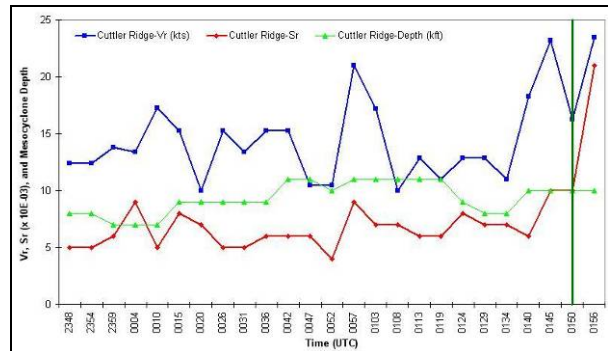


Fig. 14. Cutler Ridge mesocyclone, 2348 UTC 1 Jun 2007-0156 2 Jun 2007. V_r , S_r , and mesocyclone depth.

3.4 Discriminator Analysis

As defined above, several discriminators were evaluated to determine their utility in cell identification. Of those evaluated in this study, only DVL showed any consistency with identifying potential severe cells.

At each volume scan, for each mesocyclone, an attempt was made to identify and locate a VES. All except the shallow Big Pine mesocyclone showed a VES at some point. However, a VES existed in only about half the volume scans on average for all mesocyclones, and only for five volume scans in the Sugarloaf mesocyclone. The Everglades, Card Sound, and Cutler Ridge mesocyclones all showed a VES for eight volume scans or more at one point, with an average magnitude of 28 m s^{-1} . The Cutler Ridge mesocyclone displayed a VES signature at the time of tornado occurrence.

Only the Cutler Ridge mesocyclone showed any distinct SW signature, with grouping of maximum values coincident with the mesocyclone. An expansion of the SW field was noted in the vicinity of the Card Sound mesocyclone. However, the SW field was noisy with all mesocyclones, and at most times there was no association of SW with mesocyclone intensity or location. This lies in contrast to Spratt et al. (1997) and Pfof (2002).

Of the discriminators investigated in this study, the DVL fields provided the most utility. DVL values above 10 kg m^{-2} identified all five mesocyclones, with values above 15 kg m^{-2} found at some point in all mesocyclones with the exception of Big Pine. In Figure 15, the Everglades and Card Sound mesocyclones stand out in the DVL field with maximum DVL values greater than 20 kg m^{-2} . However, the Cutler Ridge mesocyclone is not as distinguished, although there are DVL values higher than 10 kg m^{-2} near the core, and higher than the background field values. As the mesocyclone approached the KAMX radar, the values diminished. This is likely due to the mesocyclone not being sampled through a full volume scan (too close to the radar to be sampled by the higher elevation slices).

Figure 16 shows the DVL field for the Sugarloaf mesocyclone. The Sugarloaf mesocyclone is showing values above 15 kg m^{-2} , while a large area of 10 kg m^{-2} values associated with the remnants of the Big Pine mesocyclone is to the northeast of Sugarloaf Key. The lighter area north of Key West is below 10 kg m^{-2} .

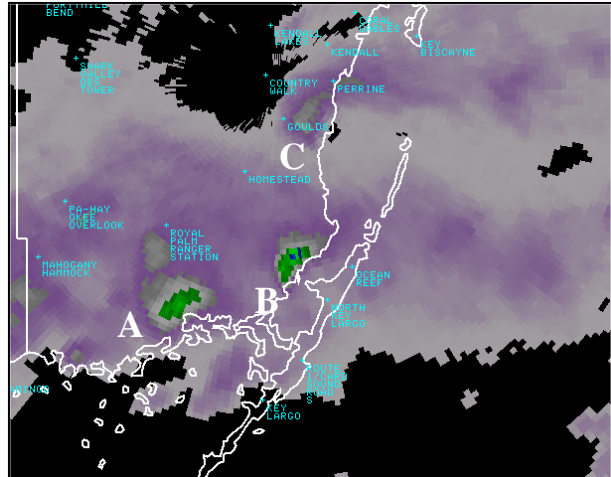


Fig. 15. KAMX DVL, 0140 UTC 2 Jun 2007. A- Everglades, B-Card Sound, C-Cutler Ridge.

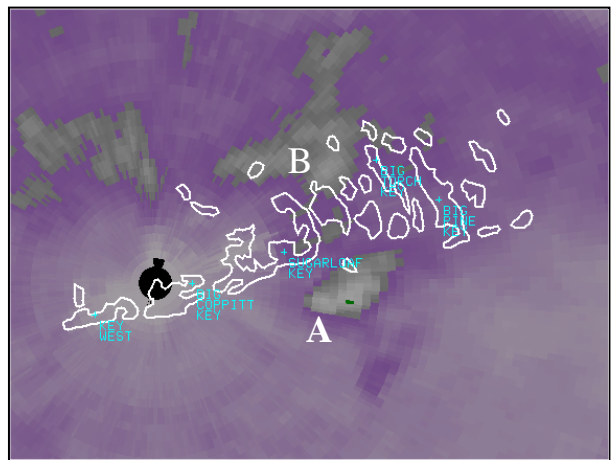


Fig. 16. KBYX DVL, 1630 UTC 1 Jun 2007. A- Sugarloaf, B-remnants of Big Pine mesocyclone.

4. CONCLUSIONS

The three mesocyclones for which there were no tornado reports did not differ in any substantive way from those that did produce tornadoes in this study, with the exception of the Big Pine mesocyclone, which was of short duration and shallow. However, the Big Pine mesocyclone was included in this study because the V_r and S_r at the lowest two radar elevation scans were as high as or higher than values from the other mesocyclones. Given the fact that all mesocyclones displayed similar intensity and organizational traits, and that two of the mesocyclones produced confirmed tornadoes, a decision to have issued a tornado warning for each mesocyclone would have been justified by storm-scale radar analysis.

All mesocyclones studied in this case developed near a northward-moving synoptic-scale boundary which extended eastward from a weak and fledgling tropical storm. Real-time identification of such

boundaries and diagnosis of the subsequent changes in key ingredients for tornadoes are necessary for successful anticipation and recognition of tornadic mesocyclone initiation. In well-developed tropical cyclones, the boundaries commonly of interest are the outer spiral rainbands. However, in less organized tropical cyclones, boundaries may be less defined and more difficult to identify. We agree with Edwards and Pietrycha (2006) that “detailed and frequent surface mesoanalysis – especially by hand, but also utilizing automated objective analysis tools – is critical to improved diagnosis of a tornado-favoring environment within the broader tropical cyclone envelope”.

This case study underscores the importance of comprehensive storm-scale radar analysis and manual techniques for discerning shallow tornadic mesocyclones. A composite approach is desirable during the radar interrogation and warning decision process in order to identify and follow the small radar features often associated with tropical cyclone tornadic cells. Emphasis should be placed on V_r , S_r , and mesocyclone depth and duration, and the temporal and spatial evolution of these fields. Warning threshold values of 9 m s^{-1} for V_r and 0.012 s^{-1} for S_r may be considered based on data examined herein. However, longer-duration mesocyclones analyzed cycled between weak and strong states, and at times, the mesocyclone itself was not detectable as a coherent structure. Therefore, it is critical to the warning process to continue to track mesocyclones after they appear to have weakened, and to be aware of possible mesocyclone regeneration.

Analysis of base reflectivity data at the 0.5° elevation angle revealed many of the same features identified in previous studies (e.g., Spratt et al. 1997) as important for radar interrogation of tropical cyclone-induced tornadic mesocyclones, including reflectivity maxima greater than those of surrounding cells, appendages, hooks, forward flank notches, and WERs.

In a busy radar field discriminators can be of use in identifying severe cells and adding confidence to the warning process. Based on the results of this study, a VES may add confidence to a warning decision when present. However, a VES was not always present during radar analysis, and its use as a discriminator, therefore, seems limited. DVL fields have shown some utility with values $>10 \text{ kg m}^{-2}$, but this number was derived from only the five mesocyclones in this study and not investigated in previous research. Further investigation is necessary before a specific DVL value can be used as a discriminator threshold. However, the use of DVL fields in the relative sense can be recommended. The utility of SW as a discriminator is surmised to be very low based on examination in this case. Out of the five mesocyclones in the study, only one showed any coherent SW signal coincident with the mesocyclone. The use of SW as a discriminator could not be confirmed as noted in previous studies, and

therefore no conclusions should be drawn from the absence or presence of a notable SW signal.

Finally, although not mentioned previously, VCP 12 is the preferred VCP in tropical cyclone tornado situations due to the higher temporal and vertical resolution offered, especially at lower elevations. The use of VCP 121 should be limited to those occasions where range folding may be obscuring a cell of interest.

5. REFERENCES

- Avila, L. A., 2007: Tropical cyclone report, Tropical Storm Barry (AL022007), 1-2 June 2007. 12 pp. [available online at http://www.nhc.noaa.gov/pdf/TCR-AL022007_Barry.pdf]
- Burgess, D. W., R. R. Lee, S. S. Parker, and D. L. Floyd, 1995: A study of mini supercells observed by WSR-88D radars. Preprints, *27th Conference on Radar Meteorology*, Vail, CO, Amer. Meteor. Soc., 4–6.
- Edwards, R., and A. E. Pietrycha, 2006: Archetypes for surface baroclinic boundaries influencing tropical cyclone tornado occurrence. Preprints, *23rd Conf. Severe Local Storms*, St. Louis, MO, Amer. Meteor. Soc., P8.2.
- Gentry, R. C., 1983: Genesis of tornadoes associated with hurricanes. *Mon. Wea. Rev.*, **111**, 1793–1805.
- Hagemeyer, B. C. and D. A. Matney, 1993: An examination of central Florida hybrid tornado outbreaks. Preprints, *17th Conf. on Severe Local Storms*, St. Louis, MO, Amer. Meteor. Soc., 332-226.
- Hill, E. L., W. Malkin, and W. A. Schulz Jr., 1966: Tornadoes associated with cyclones of tropical origin-practical features. *J. Appl. Meteor.*, **5**, 745–763.
- McCaul, E. W., Jr., 1991: Buoyancy and shear characteristics of hurricane-tornado environments. *Mon. Wea. Rev.*, **119**, 1954–1978.
- Novlan, D. J., and W. M. Gray, 1974: Hurricane spawned tornadoes. *Mon. Wea. Rev.*, **102**, 476–488.
- Pearson, A. D., and A. F. Sadowski, 1965: Hurricane-induced tornadoes and their distribution. *Mon. Wea. Rev.*, **93**, 461–463.
- Pfost, R. L., 2002: Unusual tornadoes associated with Hurricane Michelle. *NWA Electronic J. of Operational Meteor.*, **2002-EJ3**, 1–20.
- Schneider, D. and S. Sharp, 2007: Radar signatures of tropical cyclone tornadoes in central North Carolina. *Wea. Forecasting*, **22**, 278–286.
- Smith, J. S., 1965: The hurricane-tornado. *Mon. Wea. Rev.*, **93**, 453–459.
- Spratt, S. M., F. Alsheimer, C. Paxton, A. Sandrik, D. W. Sharp, and P. Welsh, 1997: A WSR-88D assessment of outer rainband tornadoes. *Wea. Forecasting*, **12**, 479–501.